Journal of Computational Physics 229 (2010) 1661–1680

Contents lists available at ScienceDirect

Journal of Computational Physics

journal homepage: www.elsevier.com/locate/jcp

An *h*-adaptive mesh method for Boltzmann-BGK/hydrodynamics coupling

Zhenning Cai [a], Ruo Li [b,*]

[a] School of Mathematical Sciences, Peking University, Beijing, China
[b] CAPT, LMAM and School of Mathematical Sciences, Peking University, Beijing 100871, China

ARTICLE INFO

Article history:
Received 14 January 2009
Received in revised form 29 October 2009
Accepted 30 October 2009
Available online 18 November 2009

Keywords:
h-Adaptive mesh method
Boltzmann–BGK equation
Hydrodynamics equations

ABSTRACT

We introduce a coupled method for hydrodynamic and kinetic equations on 2-dimensional *h*-adaptive meshes. We adopt the Euler equations with a fast kinetic solver in the region near thermodynamical equilibrium, while use the Boltzmann-BGK equation in kinetic regions where fluids are far from equilibrium. A buffer zone is created around the kinetic regions, on which a gradually varying numerical flux is adopted. Based on the property of a continuously discretized cut-off function which describes how the flux varies, the coupling will be conservative. In order for the conservative 2-dimensional specularly reflective boundary condition to be implemented conveniently, the discrete Maxwellian is approximated by a high order continuous formula with improved accuracy on a disc instead of on a square domain. The *h*-adaptive method can work smoothly with a time-split numerical scheme. Through *h*-adaptation, the cell number is greatly reduced. This method is particularly suitable for problems with hydrodynamics breakdown on only a small part of the whole domain, so that the total efficiency of the algorithm can be greatly improved. Three numerical examples are presented to validate the proposed method and demonstrate its efficiency.

1. Introduction

In this paper, we study a coupled method for the kinetic and hydrodynamic equations on an *h*-adaptive mesh in 2-dimensional case. In situations where the hydrodynamic equations do not provide a satisfactory description of the physical system of concern so as to require a kinetic description, we have to adopt the Boltzmann equation, or a simplified version of it, i.e. the Boltzmann-BGK equation. From a computational perspective, it is much more expensive to solve such models with a microscopic quantity resolution. In practice, many problems can be described by the continuum models on most part of the domain where the hydrodynamics breakdown only happened very locally, such as shock layers or an extremely rarefied part, where a coupled method of the continuum/kinetic models can be efficient without loss of physical correctness. There have been many investigations in this direction in the last few years; these include the coupling of different models and different implementation techniques. This paper is a further study of the method introduced in [4] on 2-dimensional *h*-adaptive meshes. As pointed out in [4,1], the Direct Simulation Monte-Carlo (DSMC) method for the Boltzmann equation is intrinsically unsteady and of low efficiency for fluids close to the thermodynamical equilibrium. Therefore, some other methods are proposed such as [20] for near continuum flows. In this paper, we followed that method in [4] to adopt the Boltzmann-BGK equation as the kinetic model instead of DSMC to reduce the computational cost on the kinetic region. The Euler equations are used as the continuum model currently and it can be smoothly extended to Navier–Stokes equations. With the buffer

* Corresponding author. Tel.: +86 10 6275 5773; fax: +86 10 6275 1801.
E-mail addresses: cai_zn1987@163.com (Z. Cai), rli@math.pku.edu.cn (R. Li).

0021-9991/$ - see front matter © 2009 Elsevier Inc. All rights reserved.
doi:10.1016/j.jcp.2009.10.050

zone method originated in [5,6] and used in [4], the coupling of the continuum model and the kinetic model can be implemented quite smoothly without the interface condition, which is often a quite delicate issue.

Using the moving buffer zone method proposed in [4], our whole computational domain is divided into three parts. At every time step, the kinetic region, where hydrodynamics could possibly break down and Boltzmann-BGK equation would need to be solved, is identified at first. This is done based on the distance from the current microscopic state to equilibrium in a certain metric space if microscopic data are available, and if not, the continuum breakdown parameter. The buffer zone is then given as a band with a prescribed width surrounding the kinetic region. The remaining part of the domain is taken as the hydrodynamic region. Both microscopic and macroscopic variables are solved in the buffer zone and the solution is the combination of both ingredients, whose proportions are determined by a cut-off function. It has been pointed out in [4] that when a fast kinetic Euler solver, such as the Perthame scheme, is used in the pure hydrodynamic region, the hydrodynamic part of the solution in the buffer zone is better to be solved by a full kinetic scheme in order to avoid oscillations. Meanwhile, the incompatibility of schemes in the buffer zone and hydrodynamic region makes it nontrivial to keep the whole scheme conservative. The loss of the conservation could introduce an observable error in the numerical solution. In our implementation, the flux for the hydrodynamic part is combined with the kinetic flux and the flux of the Perthame scheme. Their ratio gradually varies according to the continuously discretized cut-off function. With this new flux, the fast scheme on the pure fluid region is turned to be applicable [4]. Both conservation and saving of computational cost can then be achieved.

In this paper, the domain used to discretize the velocity is a disc with polar coordinates instead of the commonly used square domain (cf. [11,21,6]). The disc domain makes it convenient to implement the conservative specularly reflective boundary condition for 2-dimensional problems. It is the first time that the piecewise constant discrete distribution is upgraded to a piecewise biquadratic and globally continuous version in the polar coordinates. The piecewise biquadratic discrete Maxwellian is numerically verified to have improved accuracy. To make the globally continuous approximation of the Maxwellian feasible, we explicitly express the constraints of the microscopic state in the equations of its nodal values, and find that these constraints have the same form as those in the piecewise constant case. Thus the results in [12] can be reused. With such an approximation, only the numerical integrations in our scheme need to be revised. Mimicing the method used in the Perthame scheme, the distribution function is substituted by an alternative version [13] to get an explicit formula.

As to the time discretization, we consider both a time-split scheme and an unsplit scheme used in [6,5]. The time-split scheme is then applied on the h-adaptive meshes without any additional difficulties, while the unsplit scheme need to be modified delicately and we do not use it in our numerical tests. Using the h-adaptive method, the number of mesh cells in the hydrodynamic region is reduced while the kinetic region is resolved with a finer mesh. Currently, the indicators used in the mesh adaptation are heuristic. It is a balance of the gradient of the macroscopic variables and the difference to the equilibrium. In the pure fluid region, the cells with fast varying macroscopic variables are refined. This adaptation strategy is demonstrated to be effective in our numerical examples.

The layout of this paper is as follows: in Section 2, we introduce the basic framework of the coupled method, and in Section 3, the details of the discretization on a static mesh are presented. In Section 4, the indicators used in the mesh adaptation are discussed and the changes in the discretized scheme on h-adaptive meshes are described. We present in Section 5 three numerical examples to validate the coupled scheme on h-adaptive meshes. Some concluding remarks will be given in the final section.

2. The hybrid method of kinetic/continuum coupling models

2.1. Boltzmann-BGK equation

Consider the nondimensionalized form of Boltzmann-BGK equation (cf. [21])

$$\begin{cases} \partial_t f + \boldsymbol{v}\cdot\nabla_{\boldsymbol{x}} f = \nu(M_f - f), \\ f(\boldsymbol{x},\boldsymbol{v},0) = f_0(\boldsymbol{x},\boldsymbol{v}), \end{cases} \tag{1}$$

where $\boldsymbol{x},\ \boldsymbol{v}\in\mathbb{R}^D$, and D is the dimension of the space. The distribution f is a non-negative function of position $\boldsymbol{x}$, velocity $\boldsymbol{v}$ and time t, and ν is the collision frequency. M_f is the Maxwell distribution, or Maxwellian, which cancels the collision term $Q(f,f)$ of the Boltzmann equation. M_f can be written as

$$M_f = M_f[n,\boldsymbol{u},T](\boldsymbol{v}) = \frac{n}{(\pi T)^{D/2}}\exp\left(\frac{-|\boldsymbol{u}-\boldsymbol{v}|^2}{T}\right), \tag{2}$$

where n is the number of particles or density, which are the same as in the dimensionless form, and $\boldsymbol{u}$ and T are the mean velocity and macroscopic temperature respectively. These macroscopic quantities are related to f through the following equations

$$\begin{aligned} n &= \int_{\mathbb{R}^D} f\,\mathrm{d}\boldsymbol{v}, \quad n\boldsymbol{u} = \int_{\mathbb{R}^D}\boldsymbol{v}f\,\mathrm{d}\boldsymbol{v}, \\ E &= \int_{\mathbb{R}^D}\frac{1}{2}|\boldsymbol{v}|^2 f\,\mathrm{d}\boldsymbol{v} = \frac{1}{2}\left(n|\boldsymbol{u}|^2 + \frac{D}{2}nT\right). \end{aligned} \tag{3}$$

As in [21], v is calculated by

$$v = \frac{8nT^{1-\chi}}{5\sqrt{\pi}Kn}. \tag{4}$$

Here $Kn = \lambda_\infty/L$ is the Knudsen number, where λ_∞ is the mean free path of free stream, and L is some characteristic length. χ is a constant for a given gas.

2.2. Decomposition of the Boltzmann-BGK equation

The coupling method in 1-dimensional case has been introduced in [4,6]. We will redescribe it here for the 2-dimensional case. The key point of our method is that the Boltzmann-BGK equation is not solved on the whole computational domain, but only on some "hydrodynamics breakdown" areas where the classic Euler or Navier–Stokes equations likely to produce incorrect solutions.

Let Ω be the computational domain. Let us assume that some sub-domains of Ω, denoted by $\Omega_1, \Omega_2, \ldots, \Omega_m$, are considered as kinetic zones, i.e., the "hydrodynamics breakdown" areas. In order to realize a smooth transition between Boltzmann-BGK equation and Euler equations, a buffer zone B_i with fixed width d is created around each Ω_i, $i = 1, 2, \ldots, m$. We define a cut-off function, which is an extension of the cut-off function defined in [4], as follows:

$$h(\boldsymbol{x}, t) = \begin{cases} 1, & \text{for } x \in \Omega_i, \\ 1 - \frac{1}{d} \min\limits_{i=1,\ldots,m} \operatorname{dist}(\boldsymbol{x}, \Omega_i), & \text{for } x \in B_i, \\ 0, & \text{other}. \end{cases} \tag{5}$$

Note that each Ω_i as well as the number of kinetic zones m will change with respect to time. Then the distribution function f is decomposed into two parts

$$f_L = (1-h)f, \quad f_R = hf. \tag{6}$$

Substitute (6) into (1), we have

$$\partial_t f_L + (1-h)\boldsymbol{v}\cdot\nabla_{\boldsymbol{x}} f = (1-h)v(M_f - f) - f\partial_t h, \tag{7}$$

$$\partial_t f_R + h\boldsymbol{v}\cdot\nabla_{\boldsymbol{x}} f = hv(M_f - f) + f\partial_t h, \tag{8}$$

with initial conditions

$$f_L(\boldsymbol{x}, \boldsymbol{v}, 0) = (1 - h(\boldsymbol{x}, 0))f(\boldsymbol{x}, \boldsymbol{v}, 0), \tag{9}$$

$$f_R(\boldsymbol{x}, \boldsymbol{v}, 0) = h(\boldsymbol{x}, 0)f(\boldsymbol{x}, \boldsymbol{v}, 0). \tag{10}$$

2.3. Boltzmann-BGK/Euler coupling

The decomposition introduced in Section 2.1 implies that outside $\bigcup_{i=1}^m \Omega_i$, hydrodynamic equations indeed make sense for $M_f \approx f$. With the definition of h, we have $f_L \approx (1-h)M_f$. Substituting these two relations into (7), the collision term disappears and an equation of M_f is formed:

$$\partial_t[(1-h)M_f] + (1-h)\boldsymbol{v}\cdot\nabla_{\boldsymbol{x}} M_f = -M_f\partial_t h. \tag{11}$$

Let

$$\boldsymbol{u}_L = \boldsymbol{u}, \quad \boldsymbol{\rho}_L = (n_L, n_L\boldsymbol{u}_L, E_L)^T = (1-h)\boldsymbol{\rho}. \tag{12}$$

Multiply (11) by $\boldsymbol{m} = \left(1, \boldsymbol{v}, \frac{1}{2}|\boldsymbol{v}|^2\right)^T$ and integrate both sides with respect to $\boldsymbol{v}$ over $\mathbb{R}^2$. By the definition of M_f, we have the following equations in Eulerian form

$$\partial_t \boldsymbol{\rho}_L + (1-h)\nabla_x \cdot \int_{\mathbb{R}^2} \boldsymbol{v}\otimes\boldsymbol{m} M_f \,\mathrm{d}\boldsymbol{v} \approx -\boldsymbol{\rho}\partial_t h. \tag{13}$$

However, in order to shift smoothly from kinetic region to hydrodynamic region, we replace M_f by f in (13) over the buffer zone, where f is defined as

$$f = M_{f_L} + f_R, \tag{14}$$

and M_{f_L} is similarly defined as that of M_f, while all macroscopic variables in the definition (2) should be modified by adding a subscript "L". Note that here f and the original distribution function are not identical. With such a definition, the equations to be solved in non-kinetic regions become

$$\partial_t \boldsymbol{\rho}_L + (1-h)\nabla_x \cdot \int_{\mathbb{R}^2} \boldsymbol{v}\otimes\boldsymbol{m} f \,\mathrm{d}\boldsymbol{v} = -\boldsymbol{\rho}\partial_t h. \tag{15}$$

This formula is actually only an approximate equation if we consider f as the real distribution function. Join (8), (14) and (15) together, the coupling is completed. The initial conditions are given as

$$f_R(\boldsymbol{x}, \boldsymbol{v}, 0) = h(\boldsymbol{x}, 0) f(\boldsymbol{x}, \boldsymbol{v}, 0), \quad \rho_L(\boldsymbol{x}, 0) = \int_{\mathbb{R}^2} \boldsymbol{m}(\boldsymbol{v}) f(\boldsymbol{x}, \boldsymbol{v}, 0)\, \mathrm{d}\boldsymbol{v}. \tag{16}$$

3. Numerical method on a static mesh

In this section, we present a practicable algorithm with the capacity to determine kinetic zones automatically, and then give a conservative numerical scheme compatible with the Boltzmann-BGK/Euler coupling equations on a static mesh.

3.1. Velocity discretization

Suppose $\Sigma \in \mathbb{R}^2$ to be a bounded computational domain for velocity $\boldsymbol{v}$. Given a macroscopic state of fluid $\boldsymbol{\rho}$, if the formula (2) is used to calculate Maxwellian at each discrete velocity, then (3) cannot hold for this discrete Maxwellian. Thus the conservation of the whole scheme will be lost. In order to overcome this difficulty, the discrete velocity model proposed in [11] is employed.

It is well known that the H-Theorem (cf. [2]) implies that the Maxwell distribution M_f minimizes the entropy functional

$$\mathcal{H}(f) = \int_{\mathbb{R}^D} f \log f \, \mathrm{d}\boldsymbol{v}, \tag{17}$$

where f satisfies (3). Mimicing this property, the discrete Maxwellian can be defined consequently.

Divide the computational domain Σ into N elements. The kth element has a volume of Δv_k with its barycenter at $\boldsymbol{v}_k$, $k = 1, 2, \ldots, N$. Assume that the spatial position $\boldsymbol{x}$ and the time t are both fixed, and then the distribution function f will be only related with $\boldsymbol{v}$. The piecewise constant discrete Maxwellian is defined by

$$\mathcal{E}_{\mathcal{K}} = \arg\min_{g \in \mathbb{R}^N} \left\{ \sum_{k=1}^{N} \Delta v_k g_k \log g_k : g \geqslant 0, \ \boldsymbol{\rho} = \sum_{k=1}^{N} \boldsymbol{m}_k g_k \Delta v_k \right\}, \tag{18}$$

where

$$\boldsymbol{m}_k = \left(1, \boldsymbol{v}_k, \frac{1}{2}|\boldsymbol{v}_k|^2\right)^T. \tag{19}$$

It was proved in [11] that if the matrix $(\boldsymbol{m}_1, \boldsymbol{m}_2, \ldots, \boldsymbol{m}_N)$ has full row rank and there is at least one strictly positive vector g satisfying the conservative constraints in (18), then there exists a unique $\boldsymbol{\alpha} \in \mathbb{R}^{D+2}$ such that

$$\mathcal{E}_k = \exp(\boldsymbol{\alpha} \cdot \boldsymbol{m}_k), \quad k = 1, 2, \ldots, N, \tag{20}$$

where $\mathcal{E}_k$ is the kth component of $\mathcal{E}_{\mathcal{K}}$. The convergence of such discretization can be found in [11,12].

It remains to find out the very $\boldsymbol{\alpha}$ that forms $\mathcal{E}_k$. This can be easily done by solving a nonlinear system of $\boldsymbol{\alpha}$

$$\sum_{k=1}^{N} \boldsymbol{m}_k \exp(\boldsymbol{\alpha} \cdot \boldsymbol{m}_k) \Delta v_k = \boldsymbol{\rho}, \tag{21}$$

which will converge in only a few steps of Newton iteration with initial guess as

$$\boldsymbol{\alpha}^{(0)} = \left(\log\left(\frac{n}{(\pi T)^{D/2}}\right) - \frac{|\boldsymbol{v}|^2}{T}, \frac{2\boldsymbol{v}}{T}, -\frac{2}{T} \right)^T. \tag{22}$$

The specularly reflective boundary condition in 2-dimensional domain, especially on a curvilinear boundary, will appear in some practical problems. This kind of boundary condition is dealt with by ghost cells at the opposite side of the reflecting wall. If a boundary cell is marked as kinetic, the associated ghost cell should have a symmetric distribution function with respect to the wall. However, if a rectangle domain in velocity space is used as Fig. 1(a), some grid points could be out of the domain in the ghost cell. Therefore, a domain which is symmetric respect to all specularly reflective boundaries can make our implementation more convenient.

However, when applying the h mesh adaptation, as the elements on the curvilinear reflecting wall are refined, the out normal of these elements are changing. This makes it difficult to construct beforehand a polygonal mesh which satisfies the symmetric property stated above. To remedy this problem, the computational domain is chosen to be a disc with polar coordinates and a continuous discrete distribution function is used so that the function value on any point can be easily accessed through a simple interpolation. On such a mesh, a new method is needed to approximate the discrete Maxwellian.

Let Σ be a disc in 2-dimensional space with its center at origin and radius $v_{\max}$. In polar coordinates (r, φ), it can be expressed by

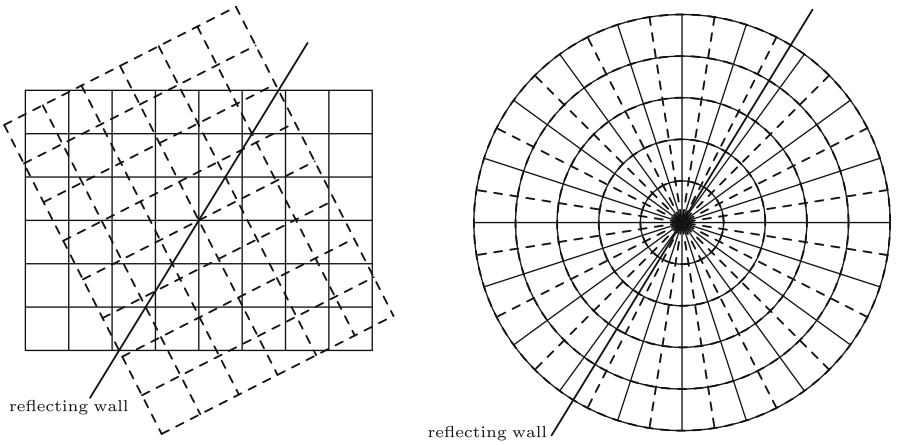

(a) Rectangle domain (b) Disc domain

Fig. 1. Meshes of velocity on the specularly reflective boundary. The solid ones indicate the boundary cells, while the dashed ones indicate the ghost cells.

$$\Sigma = \{(r,\varphi)|0 \leqslant r \leqslant v_{\max},\ 0 \leqslant \varphi < 2\pi\}. \tag{23}$$

The mesh on Σ is a uniform one such that all the grid points form a point set

$$\mathcal{V} = \{(i\Delta r, j\Delta\varphi)|i = 1,\ldots,M,\ j = 1,\ldots,N\}, \cup \{(0,0)\}, \tag{24}$$

where

$$M\Delta r = v_{\max}, \quad N\Delta\varphi = 2\pi. \tag{25}$$

Let both M and N be even. A piecewise biquadratic approximation can then be applied. The following numerical integration formula is accurate for biquadratic functions over a rectangle $[r^0, r^1] \times [\varphi^0, \varphi^1]$:

$$\int_{r^0}^{r^1} \mathrm{d}r \int_{\varphi^0}^{\varphi^1} rf(r,\varphi)\mathrm{d}\varphi = \frac{(r^1 - r^0)(\varphi^1 - \varphi^0)}{36} \sum_{i=0}^{2}\sum_{j=0}^{2} c_i c_j r^{i/2} f(r^{i/2}, \varphi^j), \tag{26}$$

where $c_0 = c_2 = 1,\ c_1 = 4$ and $r^{1/2} = (r^0 + r^1)/2$. Let $\tilde{f}$ be a continuous function on Σ, which is biquadratic on every cell $[2(i-1)\Delta r,\ 2i\Delta r] \times [2(j-1)\Delta\varphi, 2j\Delta\varphi]$ where $i = 1,\ldots,M/2$ and $j = 1,\ldots,N/2$. Then

$$\int_\Sigma \tilde{f}(\boldsymbol{v})\mathrm{d}\boldsymbol{v} = \int_\Sigma r\tilde{f}(r,\varphi)\mathrm{d}r\,\mathrm{d}\varphi = \sum_{i=1}^{M/2}\sum_{j=1}^{N/2} \int_{2(i-1)\Delta r}^{2i\Delta r} \mathrm{d}r \int_{2(j-1)\Delta\varphi}^{2j\Delta\varphi} r\tilde{f}(r,\varphi)\mathrm{d}\varphi. \tag{27}$$

According to (26), each term in the summation at the right hand side of (27) can be expressed by a linear combination of function values on nine grid points, so the whole integral turns out to be a combination of values on all grid points. Now the technique used in the piecewise constant approximation is still valid. According to our experience, this type of approximation is more robust in practical computation. On the same mesh, when Newton iteration fails for piecewise constant approximation due to the inadequate fineness of velocity mesh or too small a computational domain, piecewise biquadratic approximation may still work and provides result is with enough accuracy.

On this uniform mesh in polar coordinates, though not implemented yet, a conservative scheme for specularly reflective boundary condition on curvilinear edge is feasible, that is, the total mass will not change after reflection. It is shown in Fig. 1(b) that grid points of two meshes may not coincide, so in order to construct a conservative scheme, the continuous expression of distribution is used. The flux is also approximated based on a biquadratic form, but one important thing is to use the expression on the boundary cell while $\boldsymbol{v}\cdot\boldsymbol{n} > 0$, and to use the expression on the ghost cell while $\boldsymbol{v}\cdot\boldsymbol{n} < 0$, just like the upwind scheme. Now, after convection, the result distribution of the boundary cell is not biquadratic, but preserves conservation. Then, by applying a conservative projection, the result distribution on the boundary cell restores its biquadratic form, so the whole scheme keeps conservation.

In our implementation, for simplicity, we directly interpolates the distribution on the ghost cell to the grid of boundary cell. Therefore the conservation is not precisely accurate. Even so, the loss or gain of mass is small enough so that no significant error can be found in the numerical results.

It is shown in Section 5 that the biquadratic approximation has a high accuracy order and this method is used in our numerical experiments. For conciseness, the notations of the piecewise constant type are used when describing our algorithm below.

3.2. Kinetic schemes

We used an unstructured triangular mesh for space discretization, since this is more applicable to domains with complex shapes. Denoting the spatial domain as Ω, we revise the finite volume schemes proposed in [4] to 2-dimensional case.

3.2.1. An unsplit method

This method was originally investigated in [5] for the coupling between Boltzmann and diffusion equations. And later in [6], it was then generalized to a large class of similar problems. The kinetic part of the scheme reads

$$f_{k,i,R}^{n+1} = f_{k,i,R}^{n} + f_{k,i}^{n}(h_i^{n+1} - h_i^{n}) - \Delta t\left[\frac{1}{V_i}\sum_j h_{ij}^{n+1} l_{ij}\phi_{i,j}(f_{k,i_j}^{n}, f_{k,i}^{n}) + \nu_i^{n}(\mathcal{E}_k[\boldsymbol{\rho}^{n}] - f_{k,i}^{n})\right], \tag{28}$$

where l_{ij} is the length of the jth boundary of element i, and i_j is the index of the jth neighbour of element i. h_i and h_{ij} are the mean values of the cut-off function on the ith element and on its jth boundary, respectively. Note that h^{n+1} is obtained before applying the scheme, which will be shown later, so the scheme is explicit. The numerical flux is defined by

$$\phi_{i,j}(f_k^L, f_k^R) = \frac{1}{2}\left[(\boldsymbol{v}_k \cdot \boldsymbol{n}_{i,j})(f_k^L + f_k^R) - |\boldsymbol{v}_k \cdot \boldsymbol{n}_{i,j}|(f_k^L - f_k^R)\right], \tag{29}$$

where $\boldsymbol{n}_{i,j}$ is the unit out normal on the jth boundary of element i.

3.2.2. A time-split method

The time-split scheme is slightly modified from the one in [4]. In [4], the time-split method was employed to simplify the construction of new kinetic zones. The modification preserves this advantage while skips the calculation of discrete Maxwellian on the middle time step, and it has hardly any effects on the numerical results. Moreover, it is explained in the next section that this scheme is more compatible with the h-mesh adaptation. It reads

$$f_{k,i,R}^{n+1/2} = h_i^{n+1} f_{k,i}^{n}, \tag{30}$$

$$f_{k,i,R}^{n+1} = f_{k,i,R}^{n+1/2} - \Delta t\left[\frac{1}{V_i}\sum_j h_{ij}^{n+1} l_{ij}\phi_{i,j}(f_{k,i_j}^{n}, f_{k,i}^{n}) - \nu_i^{n}(\mathcal{E}_k[\boldsymbol{\rho}^{n}] - f_{k,i}^{n})\right]. \tag{31}$$

The first step is as a redistribution of the kinetic and hydrodynamic parts, but the total distribution of particles in velocity remains. The second step performs the convection and the collision. Details can be found in [4].

3.3. Hydrodynamic schemes

Hydrodynamic part of distribution exists in both buffer zone and pure hydrodynamic region, while different schemes are used therein.

In the buffer zone, we imitate the schemes in the previous two subsections and get the two schemes as following

- *Unsplit scheme*

$$\boldsymbol{\rho}_{i,L}^{n+1} = \boldsymbol{\rho}_{i,L}^{n} - \boldsymbol{\rho}_i^{n}(h_i^{n+1} - h_i^{n}) - \frac{\Delta t}{V_i}\sum_{k=1}^{N} \boldsymbol{m}_k \Delta v_k \sum_j (1 - h_{ij}^{n+1}) l_{ij}\phi_{i,j}(f_{k,i_j}^{n}, f_{k,i}^{n}). \tag{32}$$

- *Time-split scheme*

$$\boldsymbol{\rho}_{i,L}^{n+1/2} = (1 - h_i^{n+1})\boldsymbol{\rho}_i^{n}, \tag{33}$$

$$\boldsymbol{\rho}_{i,L}^{n+1} = \boldsymbol{\rho}_{i,L}^{n+1/2} - \frac{\Delta t}{V_i}\sum_{k=1}^{N} \boldsymbol{m}_k \Delta v_k \sum_j (1 - h_{ij}^{n+1}) l_{ij}\phi_{i,j}(f_{k,i_j}^{n}, f_{k,i}^{n}). \tag{34}$$

These two methods turn out to be ordinary kinetic schemes for Euler equations, which is denoted by $KS(\boldsymbol{\rho}_{i,L}^{n}, f^{n})$, and the computational cost is no less than the schemes in kinetic zones. For efficiency, the Maxwellain M_f is substituted by a simpler function so that the integral in the numerical scheme can be obtained analytically. The solver in one dimensional case has been proposed in [4] as the Perthame scheme, and now we extend it to the 2-dimensional case. Referring to [13], an alternative form of equilibrium function is given as

$$M(\boldsymbol{v}) = \begin{cases} \tilde{\alpha}, & |\boldsymbol{v} - \boldsymbol{u}| \leqslant \tilde{\beta}, \\ 0, & \text{others}. \end{cases} \tag{35}$$

Here $\tilde{\alpha}$ and $\tilde{\beta}$ are chosen such that if we substitute M for f in (3), the equations in (3) still hold. Thus a simple calculation gives

$$\tilde{\alpha} = \frac{n}{2\pi T}, \quad \tilde{\beta} = \sqrt{2T}. \tag{36}$$

Table 1
Accurate integral formulas.

	Case 1: $b \geqslant \tilde{\beta}$	Case 2: $\lvert b\rvert < \tilde{\beta}$
I_1	$\pi\tilde{\alpha}\tilde{\beta}^2 b$	$\tilde{\alpha}[(2\tilde{\beta}^2 + b^2)c/3 + \tilde{\beta}^2 b\theta]$
I^*	$\pi\tilde{\alpha}\tilde{\beta}^2(b^2 + \tilde{\beta}^2/4)$	$\tilde{\alpha}\left[bc(13\tilde{\beta}^2 + 2b^2)/12 + \tilde{\beta}^2(b^2 + \tilde{\beta}^2/4)\theta\right]$
I_2	$n_2 aI_1 + n_1 I^*$	$n_2 aI_1 + n_1 I^*$
I_3	$-n_1 aI_1 + n_2 I^*$	$-n_1 aI_1 + n_2 I^*$
I_4	$I_1(a^2 + b^2 + \tilde{\beta}^2)/2$	$I^{**} + \tilde{\alpha}\tilde{\beta}^2 b(\tilde{\beta}^2 + a^2 + b^2)\theta/2$

Note 1: $I^{**} = \tilde{\alpha}c(6\tilde{\beta}^4 + 23\tilde{\beta}^2 b^2 + b^4 + 5a^2 b^2 + 10a^2\tilde{\beta}^2)/30$.
Note 2: If $b \leqslant -\tilde{\beta}$, all I_j's are zero.

In the pure hydrodynamic region where $h = 0$, we have

$$\boldsymbol{\rho}_i^{n+1} = \boldsymbol{\rho}_i^n - \frac{\Delta t}{V_i}\sum_j l_{ij}\int_{\mathbb{R}^2}\boldsymbol{m}\phi_{i,j}(M_{i_j}^n, M_i^n)\,\mathrm{d}\boldsymbol{v} = \boldsymbol{\rho}_i^n - \frac{\Delta t}{V_i}\sum_j l_{ij}\left[\int_{\mathbb{R}_{i,j}^{2+}}\boldsymbol{m}(\boldsymbol{v}\cdot\boldsymbol{n}_{i,j})M_i^n\,\mathrm{d}\boldsymbol{v} + \int_{\mathbb{R}_{i,j}^{2-}}\boldsymbol{m}(\boldsymbol{v}\cdot\boldsymbol{n}_{i,j})M_{i_j}^n\,\mathrm{d}\boldsymbol{v}\right], \tag{37}$$

where $\mathbb{R}_{i,j}^{2\pm} = \{\boldsymbol{v}|\boldsymbol{v}\cdot\boldsymbol{n}_{i,j}\gtrless 0\}$.

Now we give the formulae to calculate

$$\int_{\boldsymbol{v}\cdot\boldsymbol{n}>0}\boldsymbol{m}(\boldsymbol{v}\cdot\boldsymbol{n})M(\boldsymbol{v})\,\mathrm{d}\boldsymbol{v}, \quad \boldsymbol{n}\text{ is an arbitrary unit vector}, \tag{38}$$

which are involved in the two integrals in Eq. (37). Suppose $\boldsymbol{u} = (u_1, u_2)^T$ and $\boldsymbol{n} = (n_1, n_2)^T$. Let

$$\begin{aligned} &a = u_1 n_2 - u_2 n_1, \quad b = u_1 n_1 + u_2 n_2,\\ &c = \sqrt{\tilde{\beta}^2 - b^2}, \quad \theta = \pi/2 + \arcsin(b/\tilde{\beta}), \end{aligned} \tag{39}$$

and I_j be the jth component of integral (38). The values of I_j's under different conditions are all listed in Table 1. With these analytical expressions, calculation for (37) runs significantly faster than the kinetic schemes.

With two different schemes used for the hydrodynamic part, the incompatiblity of different schemes could destroy the conservation of moments on the transitional cells if in two neighbouring elements, different schemes are used for the hydrodynamic part. As an alternative, we can force every boundary line betweens cells in the mesh to use the same type of flux in its two neighbouring elements, such that the conservation can be guaranteed. However, numerical oscillations could appear on the interface between buffer zone and pure hydrodynamic region. This phenomenon was originally mentioned in [4] and also appears in our numerical experiments. We propose the following scheme in the buffer zone to solve this problem.

$$\boldsymbol{\rho}_{i,L}^{n+1} = KS(\boldsymbol{\rho}_{i,L}^n, h^{n+1}f^n) - \frac{\Delta t}{V_i}\sum_j(1 - h_{ij}^{n+1})^2 l_{ij}\times\left[\int_{\mathbb{R}_{i,j}^{2+}}\boldsymbol{m}(\boldsymbol{v}\cdot\boldsymbol{n}_{i,j})M_i^n\,\mathrm{d}\boldsymbol{v} + \int_{\mathbb{R}_{i,j}^{2-}}\boldsymbol{m}(\boldsymbol{v}\cdot\boldsymbol{n}_{i,j})M_{i_j}^n\,\mathrm{d}\boldsymbol{v}\right], \tag{40}$$

where KS is the kinetic Euler solver (32) or (33) and (34). Here both schemes are used in the buffer zone and the proportion of the kinetic Euler solver gradually changes from 1 to 0 while transiting from pure kinetic to pure hydrodynamic region. That is to say, the buffer zone is reused as a transitional buffer between two hydrodynamic schemes. Now the whole scheme becomes conservative, that is, there is no loss or gain of mass, momentum and energy, thanks to our continuous construction of the discrete cut-off function h (detailed explanation can be found in the last two paragraphs of the next subsection). Take the time-split scheme as an example. It gives

$$\begin{aligned} \sum_i \boldsymbol{\rho}_i^{n+1}V_i &= \sum_i \boldsymbol{\rho}_{i,R}^{n+1}V_i + \sum_i \boldsymbol{\rho}_{i,L}^{n+1}V_i = \sum_i\sum_k \boldsymbol{m}_k f_{k,i,R}^{n+1}\Delta v_k V_i + \sum_i \boldsymbol{\rho}_{i,L}^{n+1}V_i\\ &= \sum_i\sum_k \boldsymbol{m}_k\left\{h_i^{n+1}f_{k,i}^n V_i - \Delta t\left[\sum_j h_{ij}^{n+1}l_{ij}\phi_{i,j}(f_{k,i_j}^n, f_{k,i}^n) - \nu_i^n(\mathcal{E}_k[\boldsymbol{\rho}_i^n] - f_{k,i}^n)\right]\right\}\Delta v_k\\ &\quad + \sum_i\left\{(1 - h_i^{n+1})\boldsymbol{\rho}_i^n V_i - \Delta t\left[\sum_k \boldsymbol{m}_k\Delta v_k\sum_j(1 - h_{ij}^{n+1})h_{ij}^{n+1}l_{ij}\phi_{i,j}(f_{k,i_j}^n, f_{k,i}^n)\right]\right\}\\ &\quad - \sum_i \Delta t\sum_j(1 - h_{ij}^{n+1})^2 l_{ij}\left[\int_{\mathbb{R}_{i,j}^{2+}}\boldsymbol{m}(\boldsymbol{v}\cdot\boldsymbol{n}_{i,j})M_i^n\,\mathrm{d}\boldsymbol{v} + \int_{\mathbb{R}_{i,j}^{2-}}\boldsymbol{m}(\boldsymbol{v}\cdot\boldsymbol{n}_{i,j})M_{i_j}^n\,\mathrm{d}\boldsymbol{v}\right]. \end{aligned} \tag{41}$$

Using

$$\sum_k \boldsymbol{m}_k\mathcal{E}_k[\boldsymbol{\rho}_i^n]\Delta v_k = \sum_k \boldsymbol{m}_k f_{k,i}^n\Delta v_k = \boldsymbol{\rho}_i^n, \tag{42}$$

Eq. (41) becomes

$$\sum_i \boldsymbol{\rho}_i^{n+1} V_i = \sum_i \boldsymbol{\rho}_i^n V_i - \Delta t \sum_i \sum_j l_{ij}(F_{i,j}^1 + F_{i,j}^2 + F_{i,j}^3), \tag{43}$$

where

$$F_{i,j}^1 = h_{ij}^{n+1} \sum_k \boldsymbol{m}_k \phi_{i,j}(f_{k,i_j}^n, f_{k,i}^n)\Delta v_k, \tag{44}$$

$$F_{i,j}^2 = (1 - h_{ij}^{n+1}) h_{ij}^{n+1} \sum_k \phi_{i,j}(f_{k,i_j}^n, f_{k,i}^n)\Delta v_k, \tag{45}$$

$$F_{i,j}^3 = (1 - h_{ij}^{n+1})^2 \left[\int_{\mathbb{R}_{i,j}^{2+}} \boldsymbol{m}(\boldsymbol{v}\cdot\boldsymbol{n}_{i,j}) M_i^n \,\mathrm{d}\boldsymbol{v} + \int_{\mathbb{R}_{i,j}^{2-}} \boldsymbol{m}(\boldsymbol{v}\cdot\boldsymbol{n}_{i,j}) M_{i_j}^n \,\mathrm{d}\boldsymbol{v} \right]. \tag{46}$$

Let $j_i \in \{1,2,3\}$ satisfies $\boldsymbol{n}_{i,j} = -\boldsymbol{n}_{i_j j_i}$. Then the j_ith neighbour of the i_jth element must be the ith element. Since h is continuous and $\boldsymbol{n}$ is the out unit normal vector, it is obvious that

$$h_{ij}^{n+1} = h_{i_j j_i}^{n+1}, \quad \mathbb{R}_{i,j}^{2\pm} = \mathbb{R}_{i_j j_i}^{2\mp}. \tag{47}$$

Thus,

$$F_{i,j}^s = -F_{i_j j_i}^s, \quad s = 1,2,3. \tag{48}$$

This equality indicates that the whole scheme is conservative. Due to the smooth transition in the buffer zone, numerical oscillations disappear.

3.4. Moving kinetic zones

For the method on a static mesh, it remains to update the cut-off function h at every time step. This is done by identifying the kinetic zones and then constructing h its definition (5).

In the kinetic regions, the distribution of particles is known so the difference between the discrete distribution and the discrete Maxwellian can be obtained directly. The pointwise indicator suggested in [4] is

$$\beta_i = \min_{k=1,\ldots,N} f_{k,i}/\mathcal{E}_k[\boldsymbol{\rho}_i] \tag{49}$$

on the ith element. If β_i is not close enough to 1, the ith element is identified as kinetic. We also consider another similar indicator, which is the L^1 norm of the difference between the discrete distribution and the discrete Maxwellian

$$\tilde{\beta}_{M,i} = 1 - \frac{1}{n}\sum_{k=1}^{N} |f_{k,i} - \mathcal{E}_k[\boldsymbol{\rho}_i]|\Delta v_k. \tag{50}$$

In our numerical experiments detailed in Section 5, it is observed that these two indicators have different behaviors. In high density region where the major non-equilibrium area lies in shocks, β_i can effectively detect the shock while $\tilde{\beta}_{M,i}$ gives a relatively poorer detection. However, if non-equilibrium is caused by rarefaction of gas, the performance of $\tilde{\beta}_{M,i}$ can be better since the quantity of discrete distribution can be very small at some velocity nodes far from the mean velocity.

It is much more difficult to make decisions out of the kinetic region where the microscopic data are unavailable. In such cells, we employ the continuum breakdown parameter proposed in [17]. This parameter has been widely used in various approaches to hybrid particle-continuum, e.g. [15,14]. The parameter reads

$$Kn_{\max} = \max\{Kn_n, Kn_T, Kn_V\}, \tag{51}$$

where

$$Kn_Q = \lambda \frac{|\nabla Q|}{Q}, \quad Q \in \{n, T, V\}, \tag{52}$$

and λ is the mean free path. The elements where $Kn_{\max}$ are bigger than a previously given threshold are shifted into kinetic region. The threshold depends on the problem under consideration. We note that there are other indicators for kinetic identification, for example the one proposed in [19]. It defines a thermal non-equilibrium indicator as

$$P_{\mathrm{Tne}} = \left| \frac{T_{\mathrm{Tr}} - T_{\mathrm{R}}}{T_{\mathrm{Tr}}} \right| \tag{53}$$

where T_{Tr} and T_{R} are the translational and rotational temperature, respectively. If P_{Tne} is large enough, the hydrodynamic equations could probably break down.

With the criteria given above, each cell in the triangulation can be identified as either kinetic or not kinetic. The cut-off function h is set to be 1 on all kinetic cells. By definition (5), the value of h over all the domain is then given. As explained in [6], although the hybrid model with an interface has been implemented through a half-flux algorithm in [3,16], the buffer zone is indeed useful since it is not clear yet what the limit of the solution is as the width of the buffer zone tends to zero.

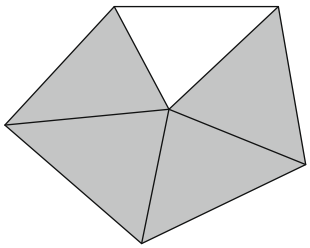

Fig. 2. The case that an element which is not marked may also have $h_i = 1$.

Since h is a distance function to the kinetic region, it is more natural to approximate it by a piecewise linear and continuous function on the spatial mesh than by a piecewise constant one. The discrete cut-off function is then given by the distance from all mesh points to the kinetic zone. Instead of carrying out an accurate and complicated calculation of the distance from all grid points to the kinetic region, we extend the kinetic zone layer-by-layer by making use of the connections of the grid points. While extending the area, the distances from the grid points to the kinetic region are consequently obtained. As the band is only several times as wide as the minimal cell, the procedure will stop after a few rounds of extension. Thus the discrete cut-off function can be obtained cheaply.

In the finite volume scheme, the mean value of h on the ith element, denoted as h_i, is used. Note that the element with $h_i = 1$ may not be an element marked as "kinetic". For example, in Fig. 2, gray elements are marked as "kinetic" while the only white area is not. However, since all the three vertices of the white element belong to other marked elements, the values on these vertices will be all set to 1. Thus on the white element, which is not marked, h_i is forced to be 1 owing to a piecewise linear form of h. Such case happens very occasionally and has no essential effect on the efficiency of the algorithm.

4. Mesh adaptation

We expect the coupled method's use of the hydrodynamic solver on most of the computational domain to achieve high efficiency. The sizes of mesh cells in the kinetic region and the hydrodynamic region should surely be different. Since the kinetic region, where physically incorrect phenomenon is most likely to appear, is the main source of numerical errors, such a region needs be further refined. Meanwhile, the solution structures in the hydrodynamic region are relatively simple. The h-adaptive method, with local refinement and coarsening of the mesh, is currently under consideration here. The h-adaptive method is to refine or coarsen a part of the mesh cells based on an indicator, which is generally a quantity related with the local error of the numerical solutions. The often adopted indicator is a *a posterior* error estimate. When the rigid error estimate is not available, certain heuristic quantity based on an understanding of the solution is also acceptable. We introduce the indicator used in our implementation at first and then discuss the changes of the numerical scheme which can work on the adaptive meshes. The changes on the numerical scheme, though slightly, is necessary.

4.1. Indicator for mesh adaptation

On each element of the space mesh, the integral of the gradient of pressure and the integral of cut-off function h are used as the indicators for mesh adaptation. The first quantity is used to indicate the magnitude of the local variation of the macroscopic variables, and the latter adds additional adjustments in the kinetic zones. The bigger one is chosen as our indicator. More precisely, the indicator on the ith element Δ_i is defined as

$$I_i = \max\left\{\int_{\Delta_i} h(\boldsymbol{x})\mathrm{d}\boldsymbol{x},\ sV_i\sum_j \frac{|p_i - p_{i_j}|}{|\boldsymbol{x}_i - \boldsymbol{x}_{i_j}|}l_{ij}\right\}, \tag{54}$$

where $\boldsymbol{x}_i$, p_i are the barycenter and mean pressure of Δ_i, respectively, and s is an appropriately selected scaling coefficient which makes the quantity of the second term comparable with the first one. Other symbols are the same as those in (28). Note that the contact discontinuity could be missed by such an indicator since for the factors based on macroscopic variables, only the gradient of the pressure is counted.

This heuristic indicator has a very obvious physical meaning, especially when applying to problems with shocks in the solution. At most of the time, the shock width is very small compared with the scale of the whole computational domain. With mesh adaptation, the structure of shock can be resolved in detail while the cost incurred on other parts of the domain is relatively small.

4.2. Changes of the time-split method

In order to work with the h-adaptive method, Some simple changes on the time-split scheme are necessary. When a mesh is altered, $f, \boldsymbol{\rho}$ and h are all needed to be updated to the new mesh. For f, only the distributions in kinetic and buffer regions

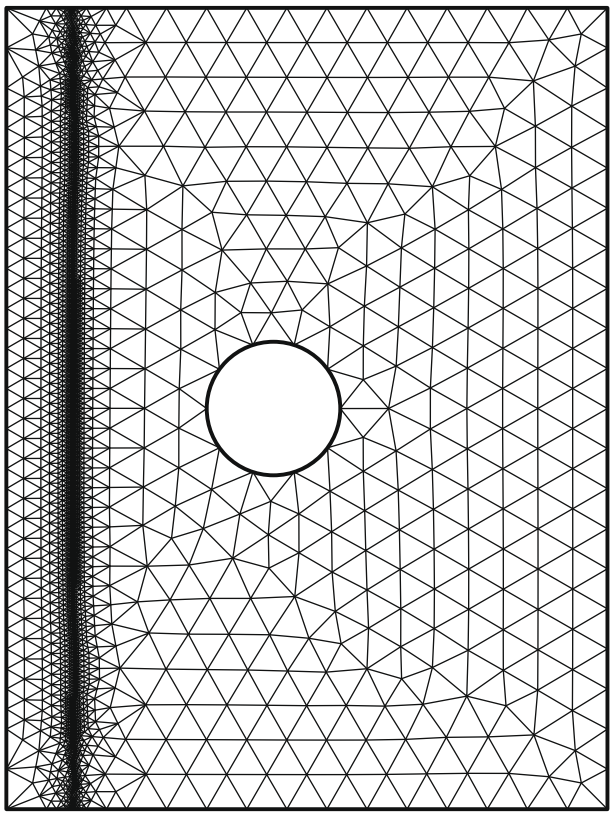

Fig. 3. The initial mesh.

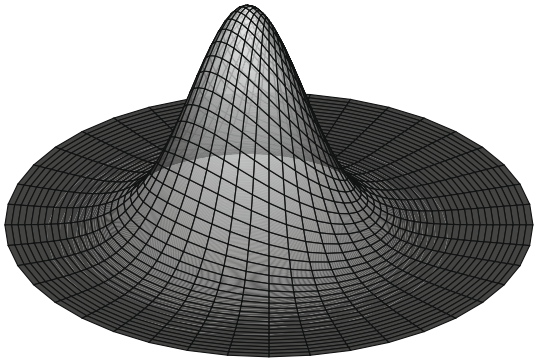

Fig. 4. A sample discrete Maxwellian.

Table 2
The approximation of Maxwellian by two different methods.

M	N	Method	$\boldsymbol{\alpha}^{(0)} - \boldsymbol{\alpha}$
20	20	Piecewise constant	(5.41e−03, −3.65e−03, −4.93e−17, 9.26e−04)
		Piecewise biquadratic	(3.47e−03, −3.97e−03, 1.17e−16, 1.37e−03)
40	40	Piecewise constant	(1.35e−03, −9.05e−04, −4.35e−17, 2.27e−04)
		Piecewise biquadratic	(3.24e−06, −1.14e−05, 3.28e−17, −7.27e−06)
80	80	Piecewise constant	(3.38e−04, −2.26e−04, −5.02e−18, 5.64e−05)
		Piecewise biquadratic	(2.05e−07, −8.40e−07, −2.38e−17, 4.15e−07)
160	160	Piecewise constant	(8.46e−05, −5.63e−05, −1.99e−17, 1.41e−05)
		Piecewise biquadratic	(−1.41e−09, 6.03e−09, 2.51e−18, −8.93e−09)

Note: M and N are defined by (25), and $\boldsymbol{\alpha}^{(0)}$ is defined by (22) which realizes Maxwellian.

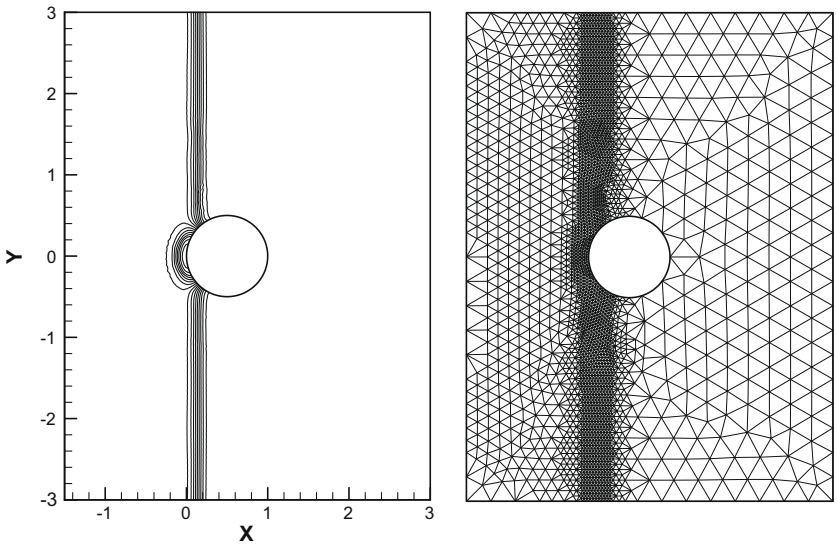

(a) Density contours (b) Computational mesh

Fig. 5. The density and mesh at $t = 0.4$.

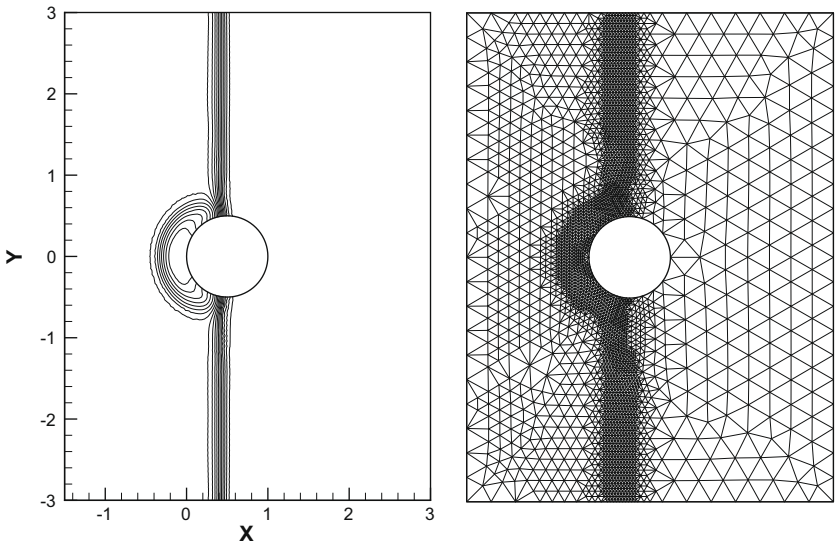

(a) Density contours (b) Computational mesh

Fig. 6. The density and mesh at $t = 0.5$.

need to be projected from old mesh to new mesh, while ρ should be updated all over the domain. So the advantage of coupling method is preserved, for the time consumed in the projection has the same order of magnitude as that in the static mesh case. The alternation is just a simple conservative projection to the new mesh. For the cut-off function, which is piecewise linear, an interpolation to the new mesh can be applied. But since the discrete cut-off function is determined only by the location of kinetic zones and the buffer width, we can simply reconstruct it without other additional costs. At most of the time, the reconstruction can be done by updating the values on only a few mesh points, and this is more accurate and faster than a piecewise linear interpolation. The algorithm for the adapting mesh is outlined as following:

1. Given an initial state $f^{(0)}$, $\rho^{(0)}$ and $h^{(0)} = 0$. Let $n = 0$.
2. Calculate h^{n+1} on the old mesh by the method we discussed in Section 3.4.
3. Calculate the indicator of mesh adaptation by (54), and then adapt the mesh.

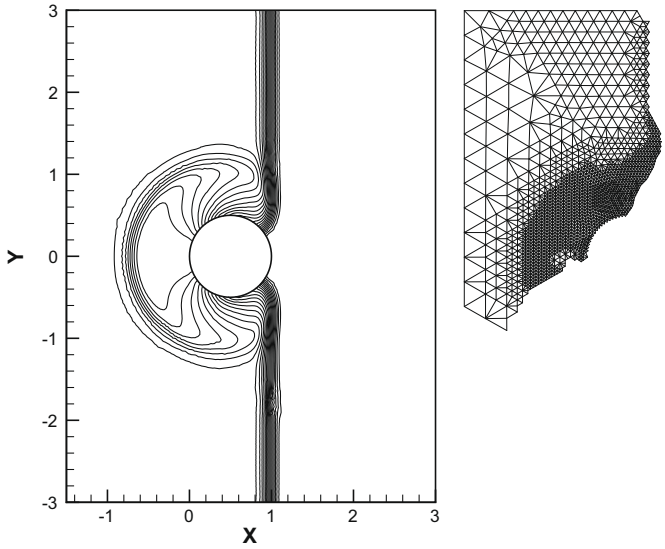

(a) Density contours

4. Project f^n and ρ^n to the new mesh, and reconstruct the cut-off function h^{n+1}.
5. Select the time step length based on the CFL condition, and apply (30), (31), (40) and (37).
6. Let $n \leftarrow n+1$ and return to step 2.

4.3. Changes of the unsplit method

It is much more difficult to make the unsplit scheme work on the adaptive meshes. The main difficulty lies in the projection of f_R and ρ_L to the new mesh which may destroy the stability of the scheme. These projections are immaterial in the time-split method. In (28), it can be seen that if the ratio $f_{k,i,R}/f_{k,i}$ is too far away from h_i, the CFL condition will not be able to guarantee the stability of the scheme. However, no theory can assure us that this ratio can be preserved after an ordinary projection. Moreover, whenever mesh cells are coarsened, this proportion can conceivably break down. For example, if $f_{i,R}/f_i = h_i$ for all i's, but h_i's are not the same, the quantity

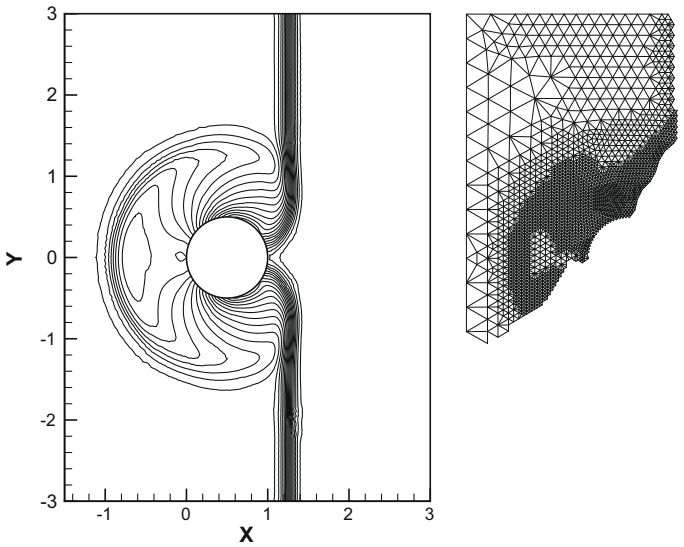

(a) Density contours

$$f_R^{\text{new}}/f^{\text{new}} = \sum_i f_{i,R} / \sum_i f_i \tag{55}$$

will not be the same as h^{new} in general. In order to overcome this difficulty, we need sophisticated processing when adapting the mesh, which slows down our computation. Since, this method is not used in our numerical experiments, we omit the details here.

5. Numerical experiments

In this section, we present three numerical examples, which are all classical benchmark problems. For simplicity, all gases we considered obey the gamma law with $\gamma = 2$, which agrees with the form of Maxwellian used in the Section 2. For a pure 2D problem, T should be replaced by $2T$ in the expression of Maxwellian. The method is implemented using C++ programming language based on the adaptive finite element package AFEPack [9]. All the computations are carried out on a desktop computer with clock speed of 2.33 GHz.

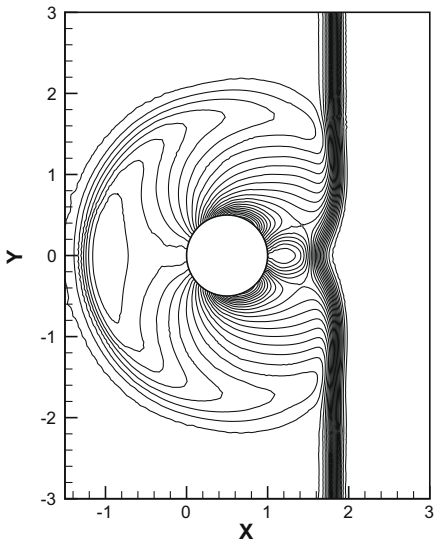

(a) Density contours

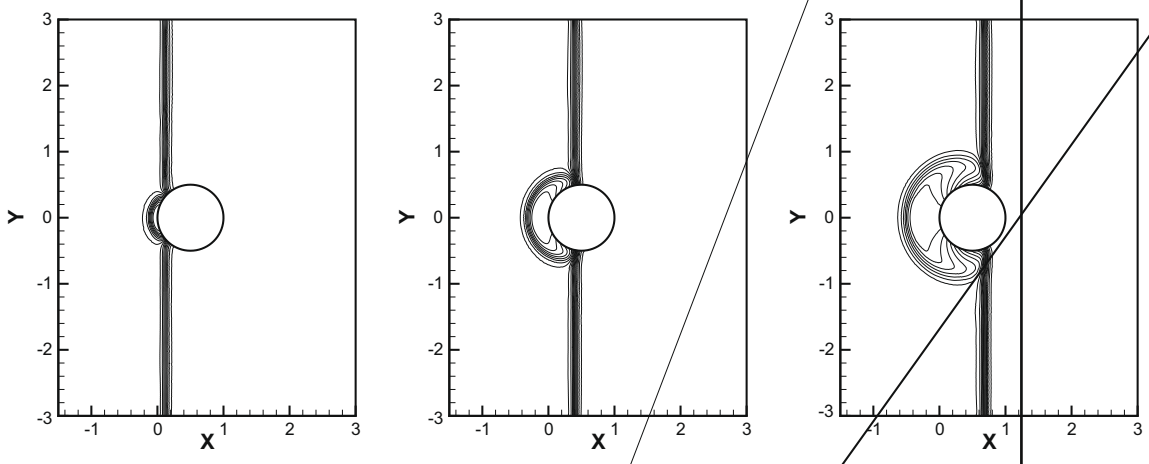

5.1. Shock diffrac

This example has
tion is unstructured, th

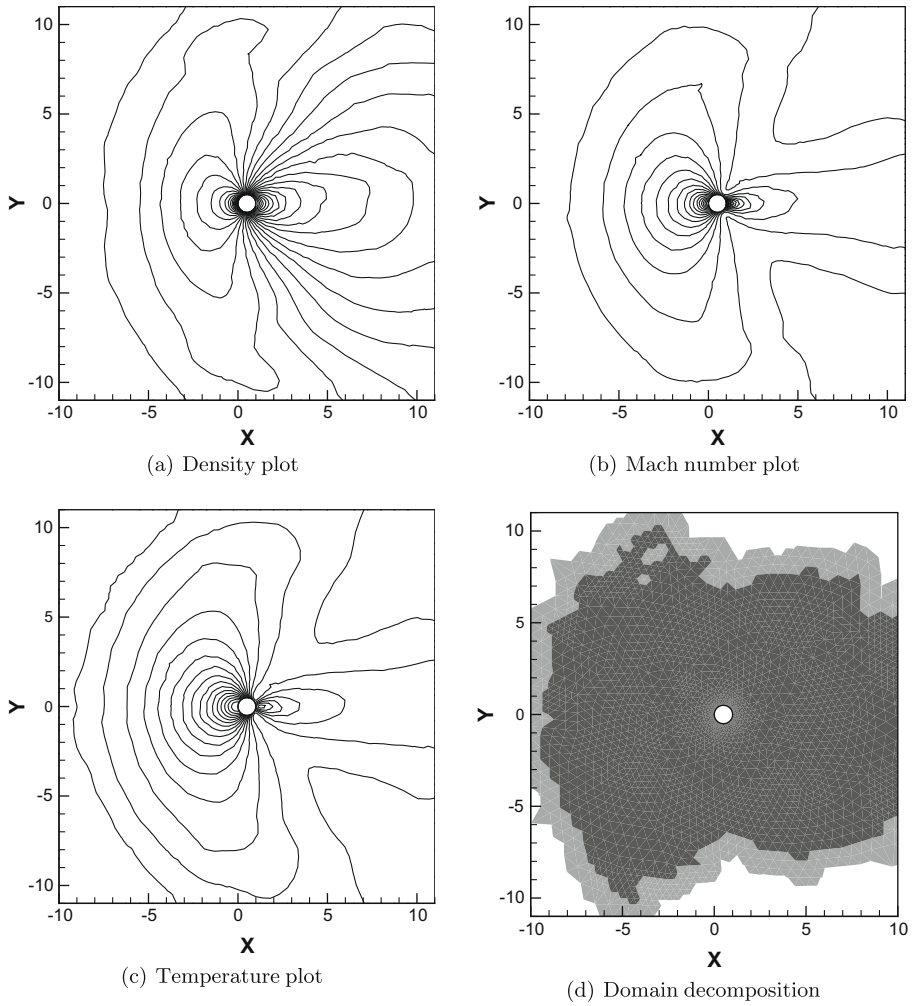

(a) Density plot (b) Mach number plot

(c) Temperature plot (d) Domain decomposition

Fig. 14. The results of the hybrid method at $t = 10.0$.

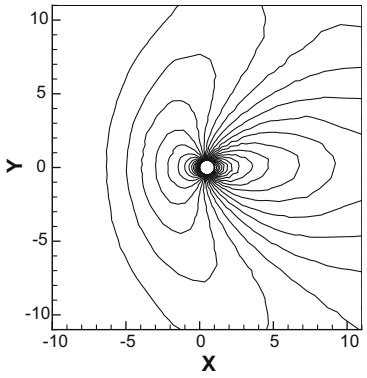

(a) Density plot

domain is set to be $[-3,5] \times [-5,5]$. The cylinder is centered at $(0.5,0)$, with a diameter of 1. The initial shock is located at $x = -1$, and the initial conditions at the undisturbed state are $n = 1,\ \boldsymbol{u} = (0,0)^T$, $T = 1$. The shock Mach number is 2.81 and the state behind shock can be obtained by the Rankine–Hugoniot condition. In this example, Maxwell gas is considered, i.e. $\chi = 1$ in (2). The freestream Knudsen number is $Kn = 0.005$.

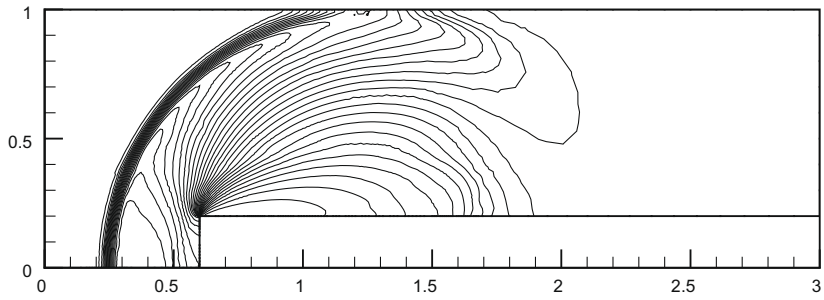

(a) $t = 0\ 4$

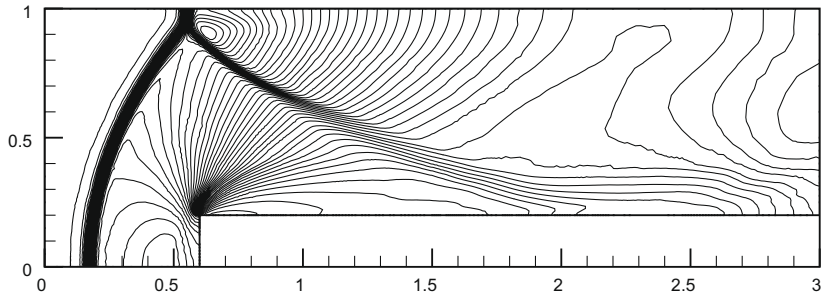

(b) $t = 0\ 8$

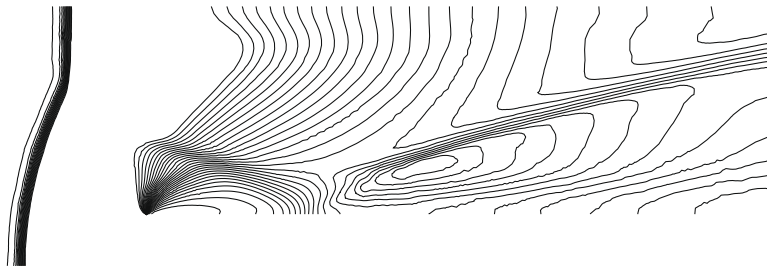

As to the boundary conditions, ghost cells are employed. The volume of ghost cells are set to be identical with the corresponding boundary cells. On the edge of the outer rectangle, the states in ghost cells are also set to be identical with that in the corresponding boundary cells. In order to test our method of processing specularly reflective boundary condition, the wall of cylinder is considered as a pure specular reflection.

Based on a very coarse background mesh, the initial mesh plotted in Fig. 3 is obtained adaptively using the indicator (54) to resolve the shock. The mesh for velocity is on a disc with $M = N = 40$. Thus the mesh includes 1600 nodes. The largest velocity, represented by the length of the radius of the largest circle, is 8. Fig. 4 shows a discrete Maxwellian, which is a continuous approximation for the discrete Maxwell distribution. In Table 2, we list the error of Maxwellian approximation in both piecewise constant and piecewise biquadratic case on sequentially refined meshes. All results are based on the macroscopic state $\rho = 1.0,\ \boldsymbol{u} = (2.0, 0.0),\ T = 1.0$ and the radius of the velocity domain is chosen as 8. From the table, it is clear that high accuracy order can be achieved by the piecewise biquadratic approximation.

Fig. 5–11 show the density contours and meshes at different times, and Fig. 12 shows the evolving of kinetic zones. From the density contours, we can see that the symmetry respect to the x-axis is well maintained, although the mesh used is unsymmetrical. The incident shock, reflecting shock, and the Mach shock can all be identified. However, the reflecting shock is not identified as kinetic, since both density and temperature are large on the shock, which makes its distribution much closer to the Maxwellian than the other two shocks. Also, the two separation points, where the gas is the most rarefied, are well captured and correctly identified as kinetic.

Let us compare this result with that in [21,6]. While noting that we compute over an area twice larger, it is fair to say that the element number, ranging from 5493 to 16551 as time develops, is much less than that in [21,6]. But our results are much

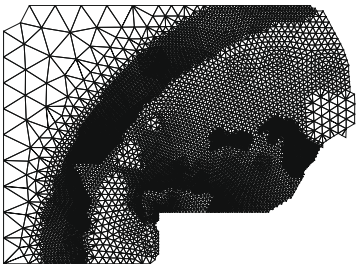

more closer to the figures in [21] than the result in [6], indicating the efficiency of the adaptive algorithm without loss of accuracy.

Additionally, for comparison, the full kinetic results are shown in Fig. 13. We simply set $h = 1$ everywhere and remove the integral of h in the adaptive indicator. Other parameters used in adaption is accordingly changed. The similarity between two results is obvious, while the full kinetic algorithm takes much longer time.

5.2. Rarefied flow past a cylinder

In this example, we consider the supersonic flow past a cylinder. The hole is also centered at $(0.5, 0)$ with a radius of 0.5, while the computational domain is set to be $[-10, 11] \times [-11, 11]$. The initial state of the flow is $(n, u_1, u_2, T) = (1.0, 1.8, 0, 1.0)$ everywhere. In order to test our method in the case of a large Knudsen number, we consider here a gas with $Kn = 1.0$.

The boundary condition at the edge of the outer rectangle is the same as that in the last example, while on the wall of cylinder, a total accommodation is applied with $T_w = 2$. The method of processing such boundary condition is the same as that in [4]. Since we use $\gamma = 2$, we cannot compare it with the practical result carried out in [10], so a full kinetic result is also exhibited for comparison. Figs. 14 and 15 show the two results at $t = 10.0$, respectively. It can be seen that the general structure of the flow is correct while the effect of the incompatibility of two schemes can also be found. In fact, our method does not show its advantage in this example since most of the computational domain is identified as kinetic.

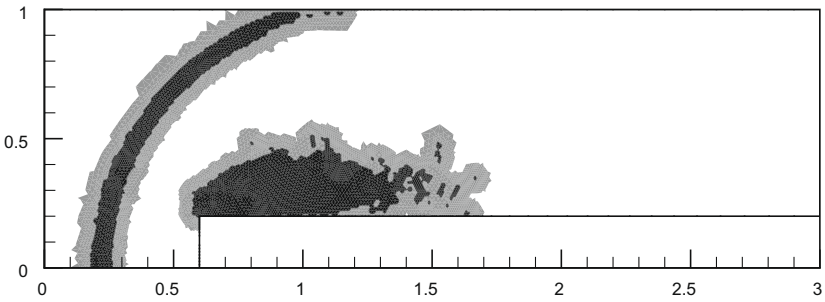

(a) $t = 0\ 4$

5.3. Forward facing step

This problem was introduced about 40 years ago in [8], and later became a commonly used test problem for fluid algorithms after [18] was published. Our settings all agree with [18] except that we set $\gamma = 2$ instead of $\gamma = 1.4$. The wind tunnel has a width of 1 on the left and 0.8 on the right, and we assume it has an infinite length while the computational domain only includes the part with $0 \leqslant x \leqslant 3$. The step height is 0.2 and located at $x = 0.6$ from the left end. Initially, the tunnel is filled with gas in an equilibrium state given by $(n, u_1, u_2, p) = (1.4, 3.0, 0.0, 1.0)$. Inflow and outflow conditions are set for the left and right boundary, respectively, and specularly reflective boundary conditions for the else. Ghost cells are also employed to process boundary conditions. Additionally, we set $Kn = 0.01$. No special treatment is applied at the step corner.

With a different γ, our results will not reproduce what has been displayed in [18]. Therefore, we use a package named AMROC [7], developed by Ralf Deiterding, which includes an example solving Euler equations for the forward facing step problem, to produce results for comparison. AMROC is an open source software that its source codes can be modified to change the value of γ. We have run AMROC's forward facing step example and use its results to validate our algorithm. However, the computation can be easily repeated so we do not present the AMROC results here.

The density contours are plotted in Fig. 16. The overall structures are in perfect agreement with that produced by AMROC, though the shocks are obviously smeared in our results. The adapted meshes are plotted in Figs. 17 and 18 shows the decomposition of computational domain. The first reflecting shock is always identified as non-equilibrium. In fact, the distribution function in this shock differs most from the Maxwellian. The second shock is also a strong one, however, the density and the temperature at the reflecting point are both big. In addition, the most rarefied part, i.e. the part above the step and near the corner, is correctly captured by the kinetic identification criteria.

6. Concluding remarks

In this paper, a 2-dimensional *h*-adaptive mesh method is developed for the Boltzmann-BGK/hydrodynamics coupling. The coupling is achieved using the buffer zone method. With a continuous cut-off function, the scheme is revised into a conservative one without loss of efficiency. The piecewise biquadratic and continuous approximation to the distribution in a disc domain can make the reflective boundary condition to be implemented conveniently with improved accuracy. The overall scheme is extended to *h*-adaptive meshes with a slight modification to the time discretization. Our current research aim on this topic is to further improve the efficiency using shifted disc for the velocity discretization with *h*-adaptive in the radius direction, and an extension of the current algorithm to 3-dimensional case.

Acknowledgments

The research of the second author was supported in part by a Foundation for the Author of National Excellent Doctoral Dissertation of PRC, the National Basic Research Program of China under the Grant 2005CB321701 and the National Science Foundation of China under the grant 10731060.

References

[1] Kazuo Aoki, Pierre Degond, Luc Mieussens, Numerical simulations of rarefied gases in curved channels: thermal creep, circulating flow, and pumping effect, Commun. Comput. Phys. 6 (5) (2009) 919–954.
[2] C. Cercignani, R. Illner, M. Pulvirenti, in: The Mathematical Theory of Dilute Gases, Applied Mathematical Sciences, vol. 106, Springer, New York, USA, 1994.
[3] N. Crouseilles, P. Degond, M. Lemou, A hybrid kinetic/fluid model for solving the gas dynamics Boltzmann-BGK equation, J. Comput. Phys. 199 (2) (2004) 776–808.
[4] Pierre Degond, Giacomo Dimarco, Luc Mieussens, A moving interface method for dynamic kinetic-fluid coupling, J. Comput. Phys. 227 (2) (2007) 1176–1208.
[5] Pierre Degond, Shi Jin, A smooth transition model between kinetic and diffusion equations, SIAM J. Numer. Anal. 42 (6) (2004) 2671–2687.
[6] Pierre Degond, Shi Jin, Luc Mieussens, A smooth transition model between kinetic and hydrodynamic equations, J. Comput. Phys. 209 (2) (2005) 665–694.
[7] Ralf Deiterding, <http://amroc.sourceforge.net/>.
[8] Ashley F. Emery, An evaluation of several differencing methods for inviscid fluid flow problems, J. Comput. Phys. 2 (3) (1968) 306–331.
[9] R. Li, W.B. Liu. <http://circus.math.pku.edu.cn/AFEPack>.
[10] G.J. Maslach, S.A. Schaaf, Cylinder drag in the transition from continuum to free-molecule flow, Phys. Fluids 6 (3) (1963) 315–321.
[11] Luc Mieussens, Discrete velocity model and implicit scheme for the BGK equation of rarefied gas dynamics, Math. Models Methods Appl. 10 (8) (2000) 1121–1149.
[12] Luc Mieussens, Convergence of a discrete-velocity model for the Boltzmann-BGK equation, Comput. Math. Appl. 41 (1–2) (2001) 83–96.
[13] B. Perthame, Boltzmann type schemes for gas dynamics and the entropy property, SIAM J. Numer. Anal. 27 (6) (1990) 1405–1421.
[14] T.E. Schwartzentruber, I.D. Boyd, A hybrid particle-continuum method applied to shock waves, J. Comput. Phys. 215 (2) (2006) 402–416.
[15] Quanhua Sun, Iain D. Boyd, Graham V. Candler, A hybrid continuum/particle approach for modeling subsonic, rarefied gas flows, J. Comput. Phys. 194 (1) (2004) 256–277.
[16] Patrick Le Tallec, François Mallinger, Coupling Boltzmann and Navier–Stokes equations by half fluxes, J. Comput. Phys. 136 (1) (1997) 51–67.
[17] Wen-Lan Wang, Iain D. Boyd, Predicting continuum breakdown in hypersonic viscous flows, Phys. Fluids 15 (1) (2003) 91–100.
[18] P. Woodward, P. Colella, The numerical simulation of two-dimensional fluid flow with strong shocks, J. Comput. Phys. 54 (1) (1984) 115–173.
[19] J.S. Wu, Y.Y. Lian, G. Cheng, R.P. Koomullil, K.C. Tseng, Development and verification of a coupled DSMC-NS scheme using unstructured mesh, J. Comput. Phys. 219 (2) (2006) 579–607.
[20] Kun Xu, Hongwei Liu, A multiple temperature kinetic model and its application to near continuum flows, Commun. Comput. Phys. 4 (5) (2008) 1069–1085.
[21] J.Y. Yang, J.C. Huang, Rarefied flow computations using nonlinear model Boltzmann equations, J. Comput. Phys. 120 (2) (1995) 323–339.